ESTABLISHMENT OF AN OPEN 3D STEAM TURBINE FLUTTER TEST CASE

D. Qi - P. Petrie-Repar -T. Gezork - T. Sun

diq@kth.se, paul.petrie-repar@energy.kth.se, gezork@kth.se

(Department of Energy Technology, Royal Institute of Technology, Stockholm, Sweden)

ABSTRACT

This paper introduces an open three-dimensional (3D) flutter test case for steam turbines. The test case is fully described and initial results are presented. The steam turbine last stage blading geometry is taken from a test case originally presented by Durham University. The stage is representative of the aerodynamic characteristics of modern steam turbine blading. To the authors' knowledge, this is the first time that a steam turbine flutter test case is presented based on an open 3D realistic blade geometry. ANSYS CFX and LUFT (Linearized Unsteady Flow solver for Turbomachinery) were both applied to calculate inviscid and RANS steady and unsteady flow solutions. Plots of aerodynamic damping versus inter-blade phase angle and plots of the local work coefficient on the blade for critical cases are presented.

KEYWORDS

FLUTTER, STEAM TURBINE, LAST STAGE, CFD, AEROELASTICITY, AEROMECHANICS

NOMENCLATURE

3D	Three dimensional
CFD	Computational Fluid Dynamics
IBPA	Inter Blade Phase Angle
LUFT	Linearized Unsteady Flow solver for Turbomachinery
N	Nodal Diameter
OEMs	Original Equipment Manufacturers
RANS	Reynolds-Averaged Navier–Stokes equations
SA	Spalart and Allmaras turbulence model
URANS	Unsteady Reynolds-averaged Navier–Stokes equations
ω^*	Reduced frequency

INTRODUCTION

Flutter is a self-excited vibration due to the interaction between the aerodynamic and structural forces. Usually, the last stage blades are the only part to be concerned with flutter risk in steam turbines (Rice et.al, 2009). These last stage blades are typically over one-meter long and are susceptible to flutter because of their low structural frequency and supersonic tip speeds. In recent years, blade flutter risk has caught more attention because of the manufacturers interest to increase turbine output and improve performance level (Rice et.al, 2009). Three-dimensional unsteady inviscid (Masserey et.al, 2012 and Rice et.al, 2009) and URANS (Stüer et.al, 2008 and Petrie-Repar et al., 2014) flow simulations for flutter analysis have been performed previously.

However, the blade profiles and the flow properties presented by OEMs are always protected and kept as a secret. These results cannot be repeated and compared with other methods. Therefore, a

flutter test case based on an open geometry for a steam turbine last stage is defined in this paper. The test case can be used by other researchers to evaluate and improve their methods.
The geometry for this test case is an open resource from Durham University, based on a generic blade, generated by Alstom Power in Rugby and modified by Durham University (Burton, 2014). The geometry was used by Durham University to provide representative inflows for exhaust hood and computational modelling of exhaust hood flows is mainly concerned in their work. It is the first time that a steam turbine flutter test case is established for an open 3D realistic blade geometry.

TEST CASE DEFINITION

The test case is based on a Durham University blade geometry (Burton, 2014), which is available online at https://www.dur.ac.uk/ecs/research/techreports/. Durham University used the geometry to define representative inflows for modelling exhaust hood flows. The turbine stage is composed of three parts in this paper, the stator, rotor and diffuser. This is different from the Durham configuration where the rotor and diffuser were considered to be one part. The schematic of the stage and boundaries are shown in Figure 1. The stage is representative for the aerodynamical characteristics of modern steam turbine. The rotor is 0.92m long and highly twisted. The stagger angle at the tip is 67 degrees. The rotor speed is 3000 rpm.
The mixing planes are the interfaces between the stator and rotor and between the rotor and diffuser to connect domains with different frames of reference (rotating and non-rotating). Two rotor domains are defined in this paper: short and long. The short rotor domain has the exit at about 0.2 chord downstream of the rotor trailing edge. The rotor and diffuser are set as one domain for long rotor domain. The definition of domains can be seen in
Figure 1.

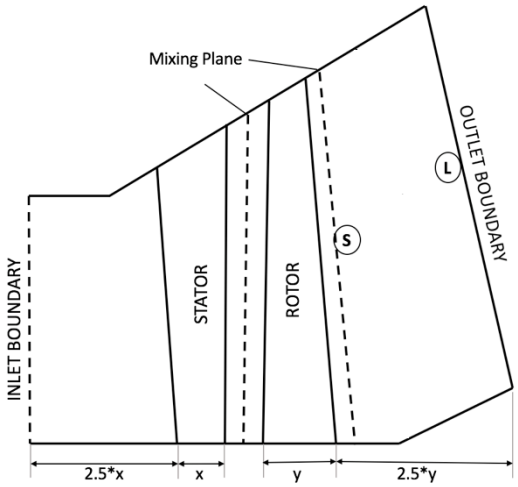

Figure 1: Schematic of stage and boundaries

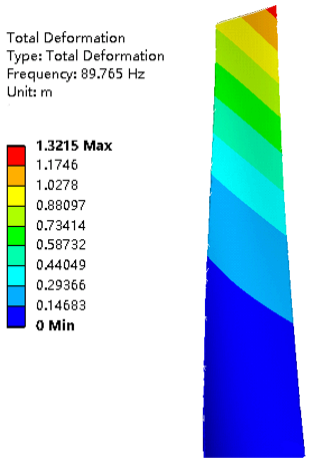

Figure 2: Mode shape

The stator inlet conditions include the representative profiles of total pressure, total temperature and three velocity components. The inlet boundary conditions are given by Alstom Power from previous multi-stage calculations and are typical for the last stage of a steam turbine and are available on the Durham website. The average inlet flow conditions are total pressure 27 kPa and total temperature 340 K. In this paper we have assumed that the incoming turbulence intensity is 10% and that the flow is fully turbulent (no transition model). The rotor outlet static pressure is 8800 Pa. The flow in the last stage is wet steam. In this paper the flow is assumed to be as ideal gas with a ratio of specific heat of 1.12 and a dynamic viscosity of $1.032 \cdot 10^{-5}$ Pa·s, which is constant over the stage. It has been shown that this assumption is valid for steam turbine flutter calculations (Petrie-Repar et al., 2014).

To obtain the blade mode, the rotor blade is assumed to be fixed at a rigid hub and the first flap bending mode is considered as the mode shape (Figure 2). The fixed hub boundary condition can be used as an approximation for blade dominated mode shapes when negligible modal coupling through the disk is present. Pre-stress and spin softening are considered in the modal analysis. The material of blade is set as titanium alloy and this is typical for a steam turbine blade. The calculated modal frequency is 89.765 Hz for the rotation speed of 3000 rpm. Subsequently, the modal frequency is modified to match reduced frequency of ω^*=0.3. Flutter onset is more likely at low reduced frequency. Thus real blades have higher frequency. The adjusted ω^* is reasonable since the modified blade geometry from Durham did not consider the structural mechanics and the calculated modal frequency is too low for the real situation. The frequency can be calculated as:

$$\mathrm{f} = \frac{\omega^* V}{2\pi c} \tag{1}$$

where f is the modal frequency. c is the chord length at mid-span. V is the average relative velocity at the turbine outlet. The modified modal frequency is 132.08 Hz.

The energy method is employed to perform the flutter analysis. The blades are assumed to be tuned and the aeroelastic eigen modes are the travelling wave mode defined by the inter blade phase angle. The Inter Blade Phase Angle (IBPA) is defined as:

$$\sigma = \frac{2\pi n}{N} \tag{2}$$

where n is the nodal diameter and N is the number of blades. The nodal diameter is the diameter formed by points which are stationary on a disk in the vibration. It is an integer and defined as:

$$-\mathrm{N}/2 \leq \mathrm{n} \leq \mathrm{N}/2 \tag{3}$$

Positive n corresponds to forward travelling waves. Negative n corresponds to backward travelling waves. The positive direction is the same direction as the blade rotation.

To determine if a certain travelling mode is stable, the unsteady work that the flow does on the blades for the prescribed travelling wave mode is calculated. The non-dimensional aerodynamic damping is calculated to determine if the rotor is at the risk of flutter. It is defined as:

$$\Xi = \frac{-W_{aero}}{\pi b \alpha^2 c^2 p_{dyn}} \tag{4}$$

where $\alpha = h_{max}/c$ and h_{max} is the maximum blade displacement, c is the chord at the mid-span, b is the blade height, p_{dyn} is the average relative total pressure at the inlet minus the average static pressure at the inlet. The normalized aerodynamic damping shows the overall stability of the blade. When the aerodynamic damping is negative, the system is not stable because the fluid flow is adding energy to the blade. Otherwise, the vibratory energy of the blade is dissipated by the flow. In order to show the local stability of the blade, the local work coefficient will be used:

$$w = \frac{-\boldsymbol{h} \cdot \hat{n} p_i}{\alpha^2 c p_{dyn}} \tag{5}$$

where h is the local displacement vector, $\hat{n}$ is the local normal vector and p_i is the imaginary component of the local unsteady pressure.

METHODS

The aim of current study is to define an open 3D test case for the realistic steam turbine blade flutter analysis. The test case is analyzed with two solvers: CFX and LUFT and two flow models: inviscid and Reynolds Average Navier-Stokes (RANS). The LUFT code is capable of performing steady-state flow simulations and linearized unsteady flow simulations. The code has been validated for flutter analysis (Petrie-Repar et al., 2006, 2007). The flow model used by the code are the 3D URANS flow equations with the Spalart and Allmaras turbulence model. The turbulence model is fully linearized for the unsteady flow simulations. A 3D non-reflecting boundary condition (Petrie-Repar, 2010) is applied at the inlet and outlet of each domain for steady and unsteady simulations, which can produce unsteady flow solutions that are independent of the far-field boundary location.

In addition, the commercial flow solver ANSYS CFX 17.0 is used. The most commonly used k-ϵ turbulence model is used and Scalable wall functions are used to calculate the boundary layer flows. ANSYS TurboGrid was used to create meshes of hexahedral cells with an O-grid around the blade. The expansion rate is used to control the number of cells for boundary layers to meet the requirement of at least 10 cells in the boundary layer for CFX (ANSYS, 2013). The detail of meshes for the cases are shown in Table 1. As LUFT does not use wall functions to resolve boundary layers, a smaller wall cell height on the walls is required.

Table 1: Detail of meshes

	Flow model	Number of nodes	Wall cell height (mm)	Minimum angle (degree)
Stator	Inviscid	367024	1	27.1695
Rotor	Inviscid	297908	1	44.33
Diffuser	Inviscid	65520	1	60.1061
CFX Stator	RANS	695304	0.1	27.1781
CFX Rotor	RANS	741264	0.1	39.9538
CFX Diffuser	RANS	90774	0.1	60.1141
LUFT Stator	RANS	877068	0.02	27.1781
LUFT Rotor	RANS	945102	0.02	41.5769
LUFT Diffuser	RANS	112914	0.02	60.011

RESULTS

Steady Computation

Steady-state simulations were performed using the ANSYS CFX and LUFT flow solvers. Two flow models were applied: inviscid flow and the Reynolds Averaged Navier-Stokes flow model. The summary of the cases and solutions is shown in Table 2. The RANS simulations were calculated on short and long rotor domains in order to investigate flow reflections at the mixing plane.

Table 2: Summary of steady state cases and solutions

Numeric tool	CFX	CFX	CFX	CFX	LUFT	LUFT	LUFT
Flow Equations	RANS	RANS	Inviscid	Inviscid	RANS	Inviscid	Inviscid
	k-ϵ	k-ϵ			SA		
Rotor Domain	Short	Long	Short	Long	Short	Short	Long
Mass flow(kg/s)	85.488	85.62	85.8975	85.904	86.42	87.04	87.07
Power (MW)	11.983	11.93	12.189	12.2117	11.62	11.92	11.96
First cell Y+	40	40	-	-	1.2	-	-
Total to static efficiency (%)	85.117	84.13	86.473	86.643	84.32	84.88	85.04

In order to compare solutions calculated by different codes and on different meshes, a standard definition of the span position is provided in the test case. The shroud is defined as 100% span and hub is defined as 0% span. As the hub line is parallel to axis and the shroud line is inclined, the span between the hub and shroud is linearly separated according to the slope of the shroud line. In other words, x% span is the conical plane that has a x% slope of the shroud line.

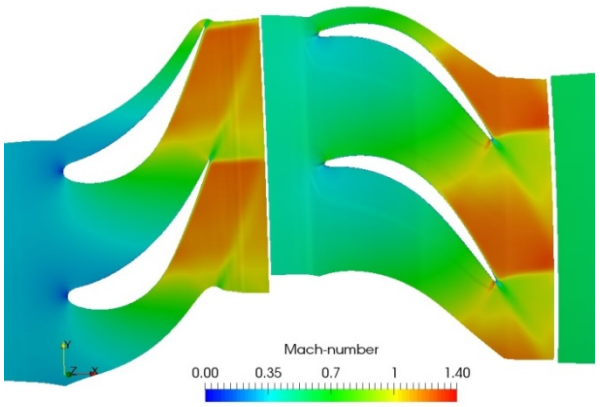

Figure 3: Relative Mach number at 50% span（LUFT）

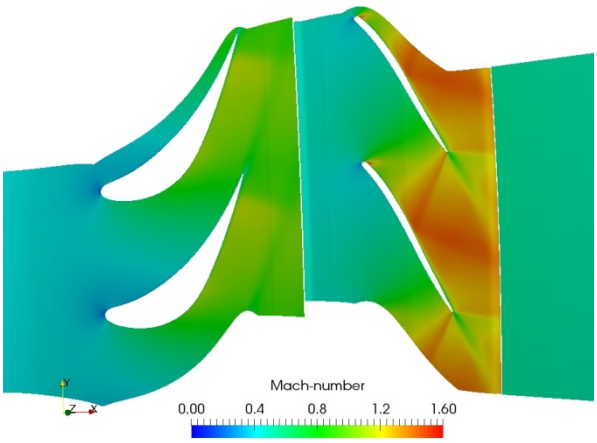

Figure 4: Relative Mach number at 90% span (LUFT)

CFX and LUFT have similar Mach number contour plots for RANS at 50% and 90% span (only LUFT solutions shown in Figure 3 and Figure 4). There are two oblique shocks starting from the rotor trailing edge. One shock forms a passage shock and the other shock extends downstream to the outlet. This shock deaccelerates the flow on the suction side. The relative Mach number at the rotor exit is mostly transonic as can be seen in Figure 8. This is a typical flow pattern for the last stage of a steam turbine.

The blade loadings at 50% and 90% span are shown in Figure 5 and Figure 6. There is an obvious difference in the blade loading at 50% span with the CFX inviscid solution and the other cases at the rotor leading edge on the suction side. The inviscid CFX simulation is run by setting the flow model to laminar, the fluid dynamic viscosity to zero and setting all wall boundaries to free-slip. This difference in the blade loading is due to flow separation at this position (Figure 7). The reason for this flow separation is unknown.

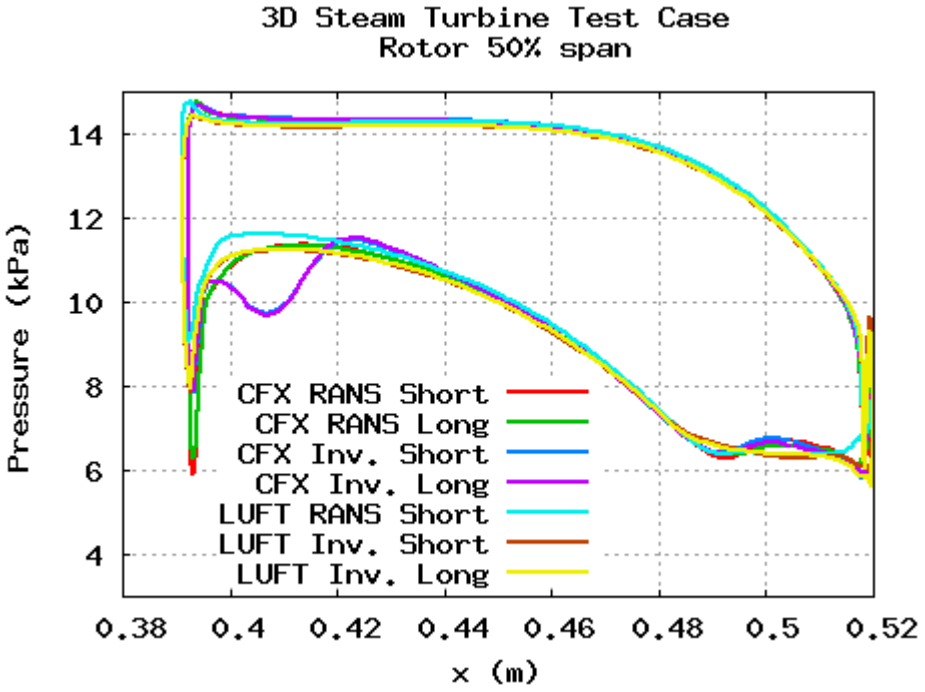

Figure 5: Blade loading on rotor at 50% span

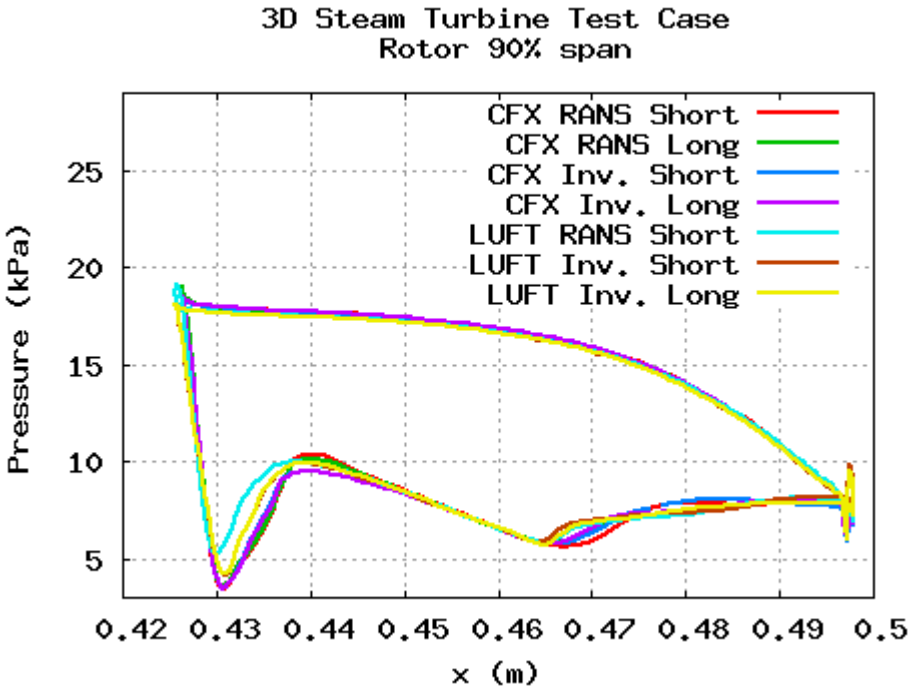

Figure 6: Blade loading on rotor at 50% span

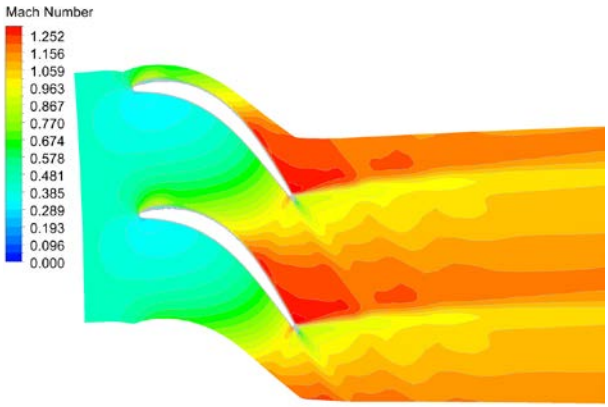

Figure 7: Relative Mach number at 50% (CFX inviscid)

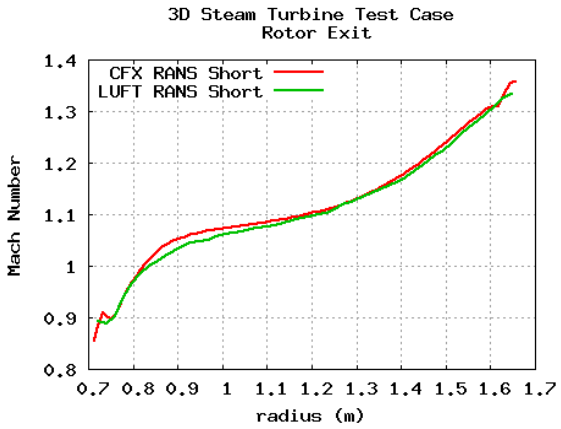

Figure 8: Relative Mach number at rotor exit

Mixing Plane

Mixing planes are used to connect the flow domains between adjacent rows when there is a difference in the rotational speed of the rows, for example the stator and the rotor. The pitchwise averaged flow properties are calculated as a function of radius either side of the mixing plane and these pitchwise average flow properties are used (after adjusting the flow by the relative rotational speed) as boundary conditions for the adjacent row. In this process, variations in the pitchwise direction are not transferred to adjacent rows as this would result in an unsteady flow perturbation at the boundary of the adjacent row and it would not be possible to calculate a steady state solution. Even though these pitchwise variations in the flow are not transferred to adjacent rows it is important that these variations are treated properly at the mixing plane to ensure that there are no unphysical flow reflections.

The LUFT code applies a steady non-reflecting boundary condition at the mixing plane to ensure that these pitchwise variations are allowed to exit the domain without reflection. The pressure

profile decay at the mixing planes for the CFX steady simulations was set to 0.0 (default 0.05). This allows the pressure profile to vary unconstrained at the mixing plane. In some cases this can lead to unstable solutions but we found that this gave the best solutions for this case. The use of the default value for this case lead to flow reflections at the mixing plane which corrupted the solution. In order to examine the flow reflections at the mixing plane, the first harmonic of the pressure in the pitchwise direction from the inviscid flow simulations at the location of the exit plane of the short rotor domain is examined. In Figure 9 the amplitude of the pressure harmonic is shown from LUFT and CFX solutions calculated with the short rotor and the long rotor domain at the location of the exit of the short rotor domain. The solutions for the short rotor domain are taken directly from the rotor exit while the solution from the long rotor is extracted at the location of the exit plane of the short rotor domain. This component of the flow is not transferred to the downstream diffuser domain. It can be seen that there is a good agreement between the LUFT and CFX solutions at this location. This suggests that the non-reflecting boundary condition is working well at the mixing plane.

Schlieren plots at 50% span for the CFX short rotor domain, CFX long rotor domain, and the LUFT short rotor domain are shown in Figures 10, 11 and 12 respectively. It can be seen that the fish tail shock at the trailing edge of the rotor is passing through the mixing plane without reflection for all solutions.

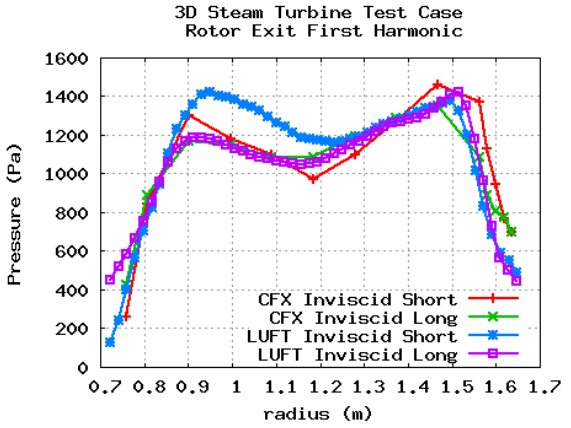

Figure 9: Amplitude of first harmonic pressure at the mixing plane

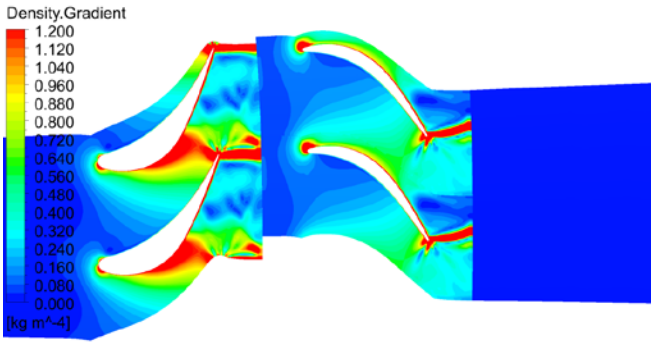

Figure 10: Schlieren plots for CFX short rotor at 50% span

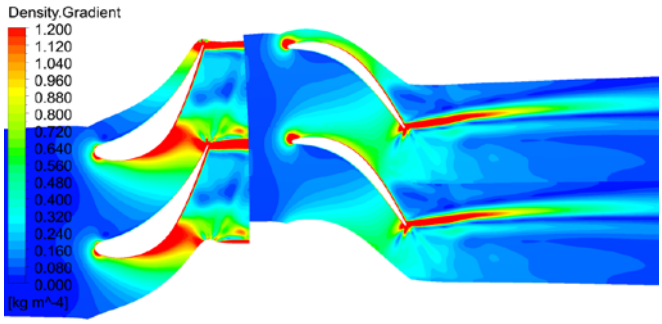

Figure 11: Schlieren plots for CFX long RANS case at 50% span

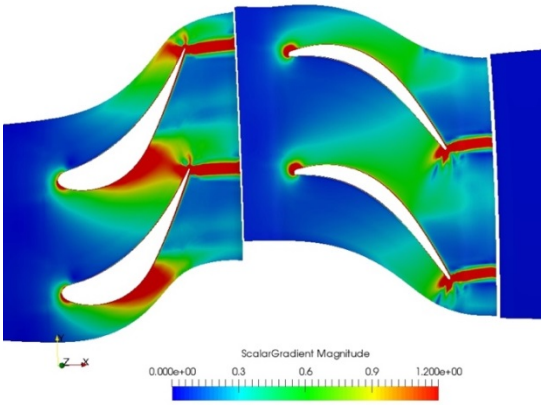

Figure 12: Schlieren plots for LUFT short RANS case at 50% span

Unsteady Computation

CFX and LUFT were used to calculate the rotor unsteady flow for different travelling wave modes. The unsteady solutions were calculated starting from steady-state solutions calculated by the same solver as the unsteady flow simulation. These unsteady simulations only included the rotor domain. For the unsteady CFX simulations, the inlet and outlet boundary profiles from the multi-row steady state results were extracted from the rotor domain to set the flow boundary conditions for the unsteady flow simulations. A steady state simulation was then run for the single rotor with extracted boundary conditions to be used as a starting point for the unsteady simulations.

The aerodynamic damping calculated by CFX and LUFT for the URANS and inviscid flow on the short and long rotor domains are shown in Figure 14. The unsteady CFX simulations were performed in the time domain as it was not possible to calculate CFX solutions with the Fourier transformation method for this case. The CFX solutions were only calculated at four IBPAs. The number of blade passages included in the CFX simulations corresponded to the minimum number of passages required for the inter-blade phase angle while using standard periodic boundary conditions, that is 1 passage for 0 degrees, 2 passages for 180 degrees and 4 passages for 90 and -90 degrees. The LUFT solutions were calculated at all possible 65 IBPAs. Overall there is a good agreement between the solutions, however, the LUFT solutions calculated on short and long domains agree better with each other while there is a greater difference between the CFX solutions.

In order to examine the solutions in more details the solutions for IBPA = -90 degree are chosen as this is the case which is closest to the least stable mode. It can been seen in Figure 13 that the damping calculated from the CFX solutions on the longer domain were higher than the other solutions. The damping versus span for IPBA = -90 degrees is shown in Figure 14. It can be seen that most of the aerodynamic work is done near the tip. The damping from the CFX longer domain solutions is clearly higher than the other solutions from 50 to 90% span. To examine this difference in more detail, the local work coefficient on the blade at 90% span on the pressure side and the suction side at IBPA = -90 degrees are shown in Figures 15 and 16. Positive local work coefficient indicates that energy is added to the blade and this is unstable. There is a good agreement between the LUFT and CFX solutions on the pressure side, however, there are significant differences in the solutions on the suction side. These difference are occurring near the leading edge and downstream of the shock at mid chord. It can be seen that the unstable work near the leading edge on the suction side predicted by the CFX solutions is significant less than the LUFT solutions. Also the amount of unstable work downstream of the shock at mid-chord on the suction side is significantly higher for the CFX short domain solutions than the other solutions. The physical reason for these differences is unknown but it may be related to unsteady flow reflections at the outlet within the CFX solutions as the CFX solver does not apply a 3D non-reflecting boundary condition at the far-field.

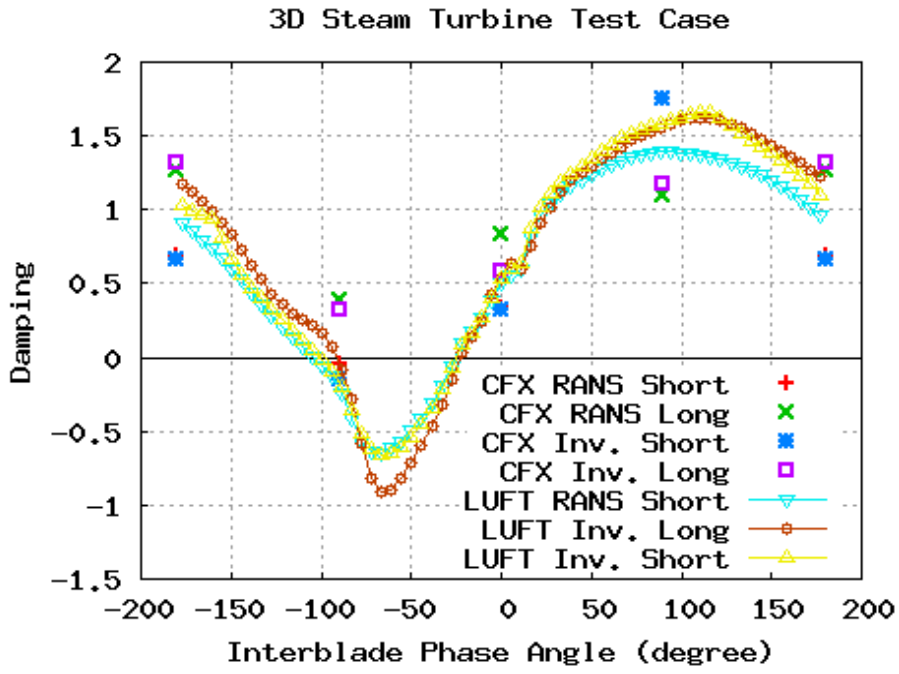

Figure 13: Normalized aerodynamic damping comparison

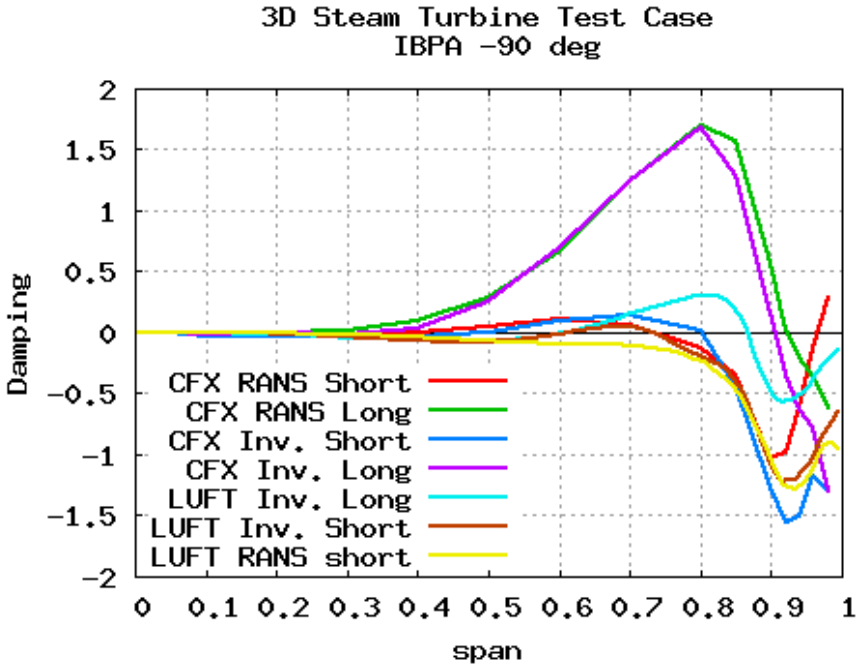

Figure 14: Local wall work density versus span for IBPA -90 degree

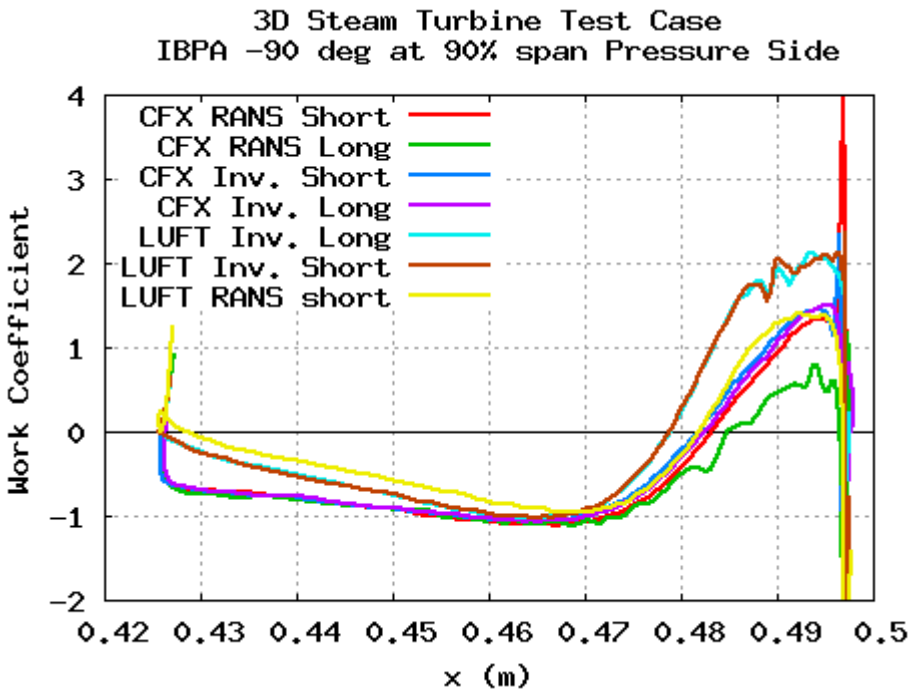

Figure 15: Local work coefficient for IBPA = -90 degrees at 90% span on pressure side

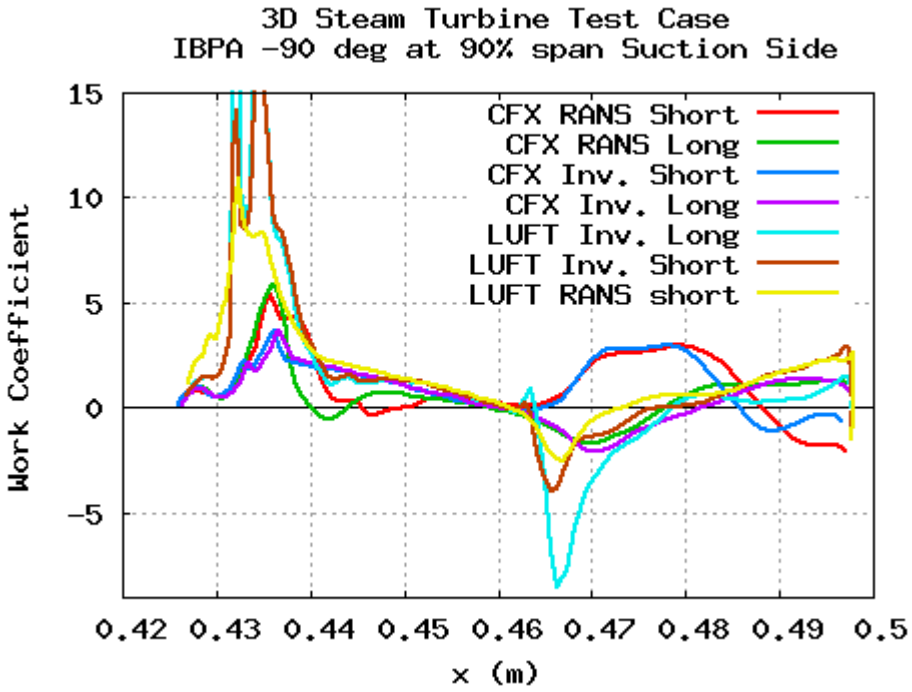

Figure 16: Local work coefficient for IBPA= -90 degrees at 90% span on suction side

DISCUSSION

At this stage, solutions for this new test case have only been calculated using two different methods and there are some differences between the solutions. Comparisons with solutions from other methods would help to develop a consensus on the correct solution. A full description of the test case and the meshes used in this paper can be found at the following website: https://www.kth.se/en/itm/inst/energiteknik/forskning/kraft-varme/ekv-researchgroups/turbomachinery-group/aeromech-test-cases/3d-steam-turbine-flutter-test-case. It is

hoped that by making this data publically available that other researchers will be encouraged to calculate solutions for the test case which they will also share with the scientific community.
The differences in the work coefficient on the suction side shown in Figure 16 may be due to reflections for the exit plane of the rotor domain. The relative Mach number of the flow at the rotor exit is high and some acoustic modes are cut-on in this region. Further work is required to determine the influence of unphysical flow reflections at the rotor exit on the calculation of the aerodynamic damping.
The test case could also be extended to include other features which are important for steam turbine blades such as the influence of shrouded blades and the effects of tip clearance. The test case could also be used to explore how various parameters affect the flutter stability for a 3D representative blade such as diffuser exit pressure, mode shape and reduced frequency. This test case could also be used to study the influence of multi-row effects on flutter as the stator row is included.
The nature blade frequency was calculated to be 89.765 Hz. This was increased to 132.08 Hz for the initial unsteady flow simulations to achieve a reduced frequency of 0.3 base on full chord as it is thought that this is more representative of actual steam turbines. Some modern steam turbines can be significantly longer and have higher stagger angles at the tip than the current test case. It would also be interesting to have another open test case for a longer blade, however, the authors are not aware of any open geometry for a longer blade.

CONCLUSION

A 3D steam turbine flutter test case has been established. The test case includes many features that are important for steam turbine flutter calculations, such as a 3D long twisted blade, transonic flow at the rotor exit, high stagger angle near the tip, mixing planes close to the blade and a blade with low natural frequency.
Initial results from two CFD methods are presented and there are some differences in the calculated solutions. There is a need for more solutions to be calculated for this test case in order to determine a consensus on the correct solution.

ACKNOWLEDGEMENTS

The financial support from China Scholarship Council for the first author is acknowledged.

REFERENCES

ANSYS. (2013). *ANSYS CFX-Solver Modeling Guide*.
Arnone, A., Benvenuti, E., (1994). *Three-dimensional Navier-Stokes analysis of a two-stage gas turbine*. Proceedings of the ASME 1994 International Gas Turbine and Aeroengine Congress and Exposition. Hague, Netherlands.
Burton, Z., (2014). Analysis of Low Pressure Steam Turbine Diffuser and Exhaust Hood Systems. PhD thesis, Durham University.
Masserey, P. A., McBean, I. and Lorini, H. (2012). Analysis and improvement of vibrational behavior on the ND37 A last stage blade. VGB Power Tech Journal (8).
Petrie-Repar, P. J., McGhee, A. M. and Jacobs, P. A. (2007). *Three-dimensional viscous flutter analysis of standard configuration 10*. Proceedings of ASME Turbo Expo 2007: Power for Land, Sea, and Air, Montreal, Canada.
Petrie-Repar, P. J., McGhee, A. M., Jacobs, P. A., and Gollan, R. (2006). *Analytical maps of aerodynamic damping as a function of operating condition for a compressor profile*. Proceedings of ASME Turbo Expo 2006: Power for Land, Sea, and Air, Barcelona, Spain.
Petrie-Repar, P. J., 2010. "Three-dimensional non-reflecting boundary condition for linearized flow solvers". In Proceedings of ASME TURBO EXPO. GT2010-23335.
Petrie-Repar, P. J. (2012). *Establishment of a steam turbine flutter test case*. Proceedings of 13th International Symposium on Unsteady Aerodynamics, Aeroacosutics and Aeroelasticity of Turbomachinery, Tokyo, Japan.

Petrie-Repar, P.J., Makhnov, V., Shabrov, N. Smirnov, E. Galaev, S. and Eliseev, K. (2014). *Advanced Flutter Analysis of A Long Shrouded Steam Turbine Blade*. Proceedings of ASME Turbo Expo 2014: Turbine Technical Conference and Exposition, Düsseldorf, Germany.

Rice, T., Bell, D. and Singh, G., (2009). Identification of the Stability Margin Between Safe Operation and the Onset of Blade Flutter. ASME. J. Turbomach. 131(1):011009.

Stüer, H., Schmitt, S., and Ashcroft, G. (2008). *Aerodynamic mistuning of structurally coupled blades*. Proceedings of ASME Turbo Expo 2008: Power for Land, Sea and Air, Berlin, Germany.